Journal of Power Sources 185 (2008) 95–103

Contents lists available at ScienceDirect

Journal of Power Sources

journal homepage: www.elsevier.com/locate/jpowsour

Modelling and analysis of a direct ascorbic acid fuel cell

Yingzhi Zeng[a], Naoko Fujiwara[b], Shin-ichi Yamazaki[b], Kazumi Tanimoto[b], Ping Wu[a,*]

[a] Institute of High Performance Computing, 1 Science Park Road, #01-01, The Capricorn, Singapore 117528, Singapore
[b] Research Institute for Ubiquitous Energy Devices, National Institute of Advanced Industrial Science and Technology (AIST), 1-8-31, Midorigaoka, Ikeda, Osaka 563-8577, Japan

ARTICLE INFO

Article history:
Received 9 April 2008
Received in revised form 26 May 2008
Accepted 12 June 2008
Available online 3 July 2008

Keywords:
Direct ascorbic acid fuel cell
Model
Dynamic simulation
Parameter estimation

ABSTRACT

L-Ascorbic acid (AA), also known as vitamin C, is an environmentally-benign and biologically-friendly compound that can be used as an alternative fuel for direct oxidation fuel cells. While direct ascorbic acid fuel cells (DAAFCs) have been studied experimentally, modelling and simulation of these devices have been overlooked. In this work, we develop a mathematical model to describe a DAAFC and validate it with experimental data. The model is formulated by integrating the mass and charge balances, and model parameters are estimated by best-fitting to experimental data of current–voltage curves. By comparing the transient voltage curves predicted by dynamic simulation and experiments, the model is further validated. Various parameters that affect the power generation are studied by simulation. The cathodic reaction is found to be the most significant determinant of power generation, followed by fuel feed concentration and the mass-transfer coefficient of ascorbic acid. These studies also reveal that the power density steadily increases with respect to the fuel feed concentration. The results may guide future development and operation of a more efficient DAAFC.

1. Introduction

Among the various types of fuel cell, systems operating at low temperature offer a number of advantages that include shorter start-up time, reduced expense on thermal insulation, and security [1,2]. The most prominent representative of this group of fuel cells is the direct methanol fuel cell (DMFC), which has received increasing attention recently due to its easy storage of the high-energy density liquid fuel and the simple reactor design that does not require fuel reforming, as is the case for classical hydrogen fuel cells [3,4]. DMFCs usually are adapted polymer electrolyte fuel cells (PEMFCs) and operate with aqueous solutions of methanol. Alternative power sources such as DMFCs and other direct-type PEMFCs are expected to be used in portable electric devices for information technology and medical equipment. However, the current fuels used in direct-type PEMFCs, namely, methanol, ethanol, propanol and ethylene glycol, are often toxic and this limits their applications in medical devices, where safety is a major concern.

Direct L-ascorbic acid (AA) fuel cells (DAAFCs) may be a solution for this problem. L-Ascorbic acid, also known as vitamin C, is an environmentally benign and biologically friendly compound. The electrochemical oxidation of ascorbic acid has been the subject of many studies on various types of electrode such as noble metals and glassy carbon [5–8]. In addition, DAAFCs offer several advantages over DMFCs [9]. For instance, the released product of DAAFCs is non-toxic, and inexpensive catalysts (e.g., carbon black) can be used for oxidation at atmospheric pressure and room temperature. While the large crossover of methanol significantly decreases the cell voltage of the DMFC [10], this problem is not serious in DAAFC as experiments show that there is very little crossover of L-ascorbic acid through a Nafion membrane of a certain thickness [9].

While the characteristics of DAAFCs have been studied by experiments and the maximum power output was found to be about one-third that of DMFCs [11], the performance of the DAAFCs can be further investigated by simulation. The performance of a DAAFC, like its counterpart DMFC, is influenced by many parameters. Investigating each parameter independently and/or all possible combinations of parameters using laboratory experiments would be costly and time-consuming. Numerical modelling of a fuel cell system is a valuable research tool for investigating system parameters that would reduce the amount of time and money required, because of the ease with which models can be modified to simulate various configurations and operating conditions. While modelling and simulation has demonstrated its importance in developing DMFCs and other chemical fuel cell systems [3,10,12–19], it remains overlooked in DAAFC development. In order to utilize DAAFCs in

* Corresponding author. Tel.: +65 64191212; fax: +65 64632536.
E-mail addresses: zengyz@ihpc.a-star.edu.sg (Y. Zeng), n-fujiwara@aist.go.jp (N. Fujiwara), s-yamazaki@aist.go.jp (S.-i. Yamazaki), tanimoto-k@aist.go.jp (K. Tanimoto), wuping@ihpc.a-star.edu.sg (P. Wu).

0378-7753/$ – see front matter © 2008 Elsevier B.V. All rights reserved.
doi:10.1016/j.jpowsour.2008.06.062

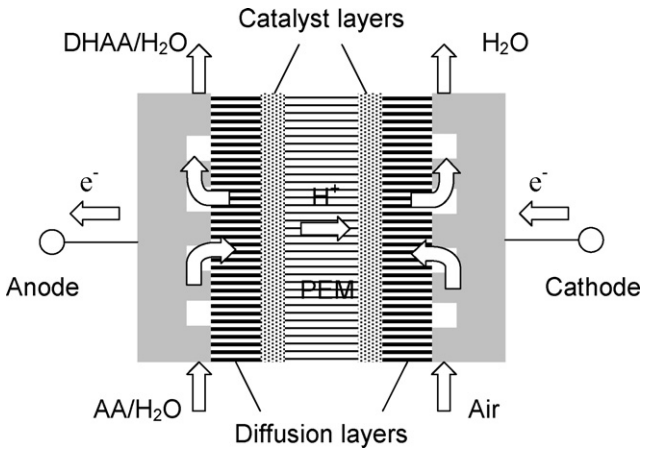

Fig. 1. Schematic diagram of the direct ascorbic acid fuel cell.

an effective way and improve their overall performance, a mathematical model is necessary so that the system can be analyzed and optimized by simulation for different operating conditions. The capability of predicting transient dynamics subject to the changes in the power demands and exterior conditions are of high interest for mobile applications. Therefore, the purpose of the present work is to develop a mathematical model for DAAFCs which allows not only studying steady-state behaviour but also investigating dynamic responses.

The proposed model is implemented in MATLAB 7.0 [20]. The model is developed on the basis of mass and charge balances, and it describes the electrochemical kinetics in the catalyst layers and the mass transfer between the bulk solutions and catalyst layers. Steady-state data from experimentally measured current–voltage curves are used for fitting the model parameters and validating the model. The dynamic behaviour of step changes and periodic changes in fuel flow rate and concentration are compared for experimental and simulated results. The sensitivity analysis of various model parameters is carried out by simulation and the most significant factors that affect power generation are discussed. These results promise to be useful for developing or operating more efficient DAAFCs.

2. Methods of approach

2.1. Experiments

A schematic diagram of the experiment set-up of the DAAFC is presented in Fig. 1. The fuel cell was fitted with a membrane electrode assembly (MEA) that consisted of a NAFION 117™ PEM in the middle, anodic and the cathodic catalyst layers on either side, diffusion layers, and the reactant distribution channels. Fuel cell experiments were performed using a single cell at atmospheric pressure and room temperature (25 °C). The parameters of the experimental set-up are summarized in Table 1.

Table 1
Experimental conditions and constants

Parameter	Description	Units	Value
U^0	Open circuit voltage	V	0.592
T	Cell operating temperature	°C	25
P_{O_2}	O_2 pressure	atm	1
A^S	Cross-sectional electrode area	m^2	10×10^{-4}
k^m	Conductivity of membrane	$\Omega^{-1}\,m^{-1}$	17
d^m	Thickness of the membrane	m	2×10^{-4}
V_a	Anode compartment volume	m^3	2.0×10^{-6}
F	Faraday constant	$C\,mol^{-1}$	96485.4
R	Gas constant	$J\,mol^{-1}\,K^{-1}$	8.3144
V_a^{CL}	Void volume of anode catalyst layer	m^3	8.0×10^{-9}
C_a	Anode capacitance	$F\,m^{-2}$	400
C_c	Cathode capacitance	$F\,m^{-2}$	500

L-Ascorbic acid was supplied as an aqueous solution to the anode, and oxygen saturated with water was fed at 100 ml min^{-1} to the cathode as the oxidant. In order to estimate the model parameters with better accuracy, the experiments were carried out by combining different levels of AA concentrations and flow rates. Specifically, the concentration was selected in the range of 0.1–1 M with the upper limit close to the AA solubility and the flow rate in the range of 1–8 ml min^{-1}, which covers the operating ranges of the DAAFC. The experiments were then performed with combinations of high, middle and low levels of concentration and high, middle and low flow rates. As a result, nine runs of experiments, as listed in Table 2, were conducted and a total of nine polarization (current–voltage) curves were measured. All experiments were carried out under galvanostatic conditions, i.e., the electrical cell current was fixed as an input variable and the resulting cell voltage was measured as an output variable.

To validate further the developed DAAFC model and gain better insight into the fuel cell performance, dynamic experiments were performed. Similar to the study of DMFC dynamics [3,10], the investigation of the dynamic behaviour of the DAAFC was undertaken by holding certain variables constant while observing other variables, e.g., the cell voltage or concentrations of reactants. Specifically, the excitation functions, i.e., step function, and periodic function of controlled variables, namely, AA feed concentration and flow rate, were applied, and the resultant responses (e.g., the resultant variation of the cell voltage with time) were measured and used to compare with the model predictions.

Table 2
Variations of experimental conditions and the resultant mass transfer coefficients

Data set #	Concentration of ascorbic acid (AA) (mol L^{-1})	AA feed flow rate (ml min^{-1})	Limiting current density readings (mA cm^{-2})	Mass transfer coefficient K^{LS} (10^{-5} m s^{-1})	Average voltage difference between the experiment and simulation (V)
1	0.5	4	95.1	1.1566	0.008
2	0.5	1	63.3	1.0820	0.011
3	0.5	8	108	1.2219	0.005
4	0.1	4	30.3	2.0539	0.012
5	0.1	8	40.0	2.4544	0.008
6	1	1	85.6	0.6045	0.010
7	1	4	122	0.6985	0.007
8	1	8	133	0.7268	0.014
9	0.2	8	90	2.8263	0.008

2.2. Assumptions of modelling

As described in Section 2.1, the basic concepts of modelling a single-cell DAAFC encompasses a PEM in the middle, the anodic and the cathodic reaction zones (catalyst layers) on both sides, and anode and cathode compartments (diffusion layers and the reactant distribution channels). Since the design configuration and working principle of the DAAFC are similar to that of a DMFC [10], similar assumptions were made as follows:

- The anode compartment is treated as a continuous stirred tank reactor (CSTR).
- Ohmic drops in current-collectors and electric connections are negligible.
- The fuel cell operates isothermally.
- Oxygen is fed in excess, i.e., oxygen conversion in the cathode compartment is negligible, and therefore no oxygen mass balance is required.
- Oxygen does not diffuse into the PEM.
- Water concentration is constant (excess component in liquid mixture).
- Mass-transport resistances in the catalyst layers are negligible.
- Mass-transport coefficients of ascorbic acid (AA) and its product dehydroascorbic acid (DHA) in the anode diffusion layer are equal.
- The mixtures in the anode compartment and in the anode diffusion layer are treated as pure liquids.

2.3. Kinetics, mass and charge balances

Experiments suggested that ascorbic acid is oxidized in the anode by a two-electron transfer reaction, i.e., the same as its metabolic conversion [11,21,22], which is described as (R1). The rate expression of the reaction takes the Butler–Volmer form, as shown by:

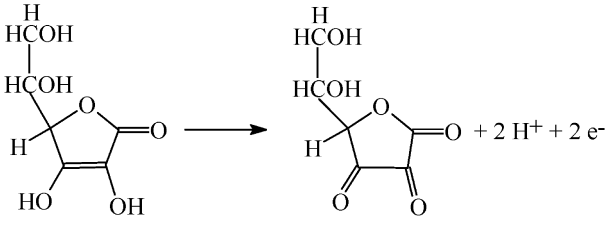

(R1)

$$r_1 = k_1^0 \exp\left(\frac{\alpha F}{RT}\eta_a\right)\left[C_{AA}^{CL} - \frac{1}{K_1}\exp\left(\frac{-F}{RT}\eta_a\right)C_{DHA}^{CL}\right] \quad (1)$$

where C_{AA} and C_{DHA} are the concentrations of AA and DHA, respectively; the superscript 'CL' indicates the catalyst layer; η_a is the anode overpotential. In addition, k_1^0 indicates the rate constant of the anode reaction at standard conditions, K_1 is the equilibrium constant, α is the charge-transfer coefficient of the anode, F is the Faraday constant, R is the gas constant, and T is the operating temperature of the cell. Notably, a reversible reaction is assumed for the AA oxidation.

In the cathode, the reduction of dissolved oxygen is described as (R2). Our preliminary study found that the reversed reaction was negligible. Thus, the reaction rate of (R2) is formulated as Eq. (2), where P_{O_2} is the oxygen partial pressure in the oxygen saturated with water at 25 °C and fed to the cathode compartment, η_c is the cathode overpotential, k_2^0 designates the rate constant of the cathode reaction at standard conditions, and β is the charge-transfer coefficient of cathode. It is noted that r_2 is defined in terms of electron generation, just like r_1 in Eq. (1).

$$0.5O_2 + 2H^+ + 2e^- \rightarrow H_2O \quad (R2)$$

$$r_2 = -k_2^0 (P_{O_2})^{1/2} \exp\left[\frac{(\beta - 1)F}{RT}\eta_c\right] \quad (2)$$

In a similar manner to the work of Sundmacher et al. [3], where the dynamics of a direct methanol fuel cell were studied, the governing equations associated with the mass balances of AA and DHA can be formulated in Eqs. (3)–(8) with the assumption that the anode is a continuous stirred tank reactor (CSTR) and functions as a storage module. In these equations, the subscripts 'a' indicates the anode compartment, the superscript 'in' the feed flow, and V_a, V_a^{CL}, Q and A^S are the volumes of the anodic compartment and catalyst layer, the AA feed flow rate, and the cross-section area of the membrane, respectively.

$$\frac{dC_{AA}}{dt} = \frac{Q}{V_a}(C_{AA}^{in} - C_{AA}) - \frac{K^{LS}A^S}{V_a}(C_{AA} - C_{AA}^{CL}) \quad (3)$$

$$\frac{dC_{DHA}}{dt} = \frac{Q}{V_a}(C_{DHA}^{in} - C_{DHA}) - \frac{K^{LS}A^S}{V_a}(C_{DHA} - C_{DHA}^{CL}) \quad (4)$$

The second terms on the right-hand side of Eqs. (3) and (4), respectively, represents the mass fluxes of AA and DHA in the anode diffusion layer where no storage is assumed. It is noted that the mass-transfer coefficient K^{LS} is taken to be equal for both AA and DHA. In the catalyst layer, the mass balances for AA and DHA in the catalyst layer are given by Eqs. (5) and (6).

$$\frac{dC_{AA}^{CL}}{dt} = \frac{K^{LS}A^S}{V_a^{CL}}(C_{AA} - C_{AA}^{CL}) - \frac{A^S}{V_a^{CL}}r_1 \quad (5)$$

$$\frac{dC_{DHA}^{CL}}{dt} = \frac{K^{LS}A^S}{V_a^{CL}}(C_{DHA} - C_{DHA}^{CL}) + \frac{A^S}{V_a^{CL}}r_1 \quad (6)$$

The charge balances at the anode and cathode are given as below where i_{cell} is the cell current density, C_a and C_c are charge double-layer capacitances of the anode and the cathode, respectively, which are measured by experiment.

$$\frac{d\eta_a}{dt} = \frac{1}{C_a}(i_{cell} - 2Fr_1) \quad (7)$$

$$\frac{d\eta_c}{dt} = \frac{1}{C_c}(-i_{cell} - 2Fr_2) \quad (8)$$

As mentioned previously, the ohmic drops in the current-collectors and electric connections are negligible. Thus the cell voltage U_{cell} can be calculated as below, where U^0 is the open-circuit

Table 3
Resultant parameter values

Symbol	Description	Unit	Value
k_1^0	Forward rate constant of AA oxidation (R1)	mol m^{-2} s^{-1}	2.91×10^{-6}
K_1	The ratio of forward rate to backward rate of AA oxidation (R1)	–	3.11×10^{-2}
k_2^0	Standard rate constant of O_2 reduction (R2)	mol m^{-2} s^{-1}	4.47×10^{-6}
α	Charge transfer coefficient of anodic reaction	–	0.410
β	Charge transfer coefficient of cathodic reaction	–	0.467

potential, and k^m and d^m are the conductivity and thickness of the membrane, respectively.

$$U_{cell} = U^0 - \eta_a + \eta_c - \left(\frac{d^m}{k^m}\right) i_{cell} \quad (9)$$

2.4. Parameter estimation

In order to make use of the developed model (Eqs. (1)–(9)) to predict the DAAFC performance, the associated parameters or constants have to be determined a priori. Some of the parameters have been measured by experiments, as shown in Table 1, while others are determined by the mathematical methods described in this section.

2.4.1. Estimation of mass-transfer coefficients

The effective mass-transfer coefficient K^{LS} is determined as follows with the measured limiting current density. In the steady-state, Eqs. (3), (5) and (7) are all zero, and the AA concentration in anode catalyst layer is also zero at limiting current. Combining Eqs. (3), (5) and (7) yields

$$K^{LS} = \frac{QI_{lim}}{2FQC^{in}_{AA} - A^s I_{lim}} \quad (10)$$

As can be seen from the above equation, in addition to the limiting current density, the mass-transfer coefficient is also affected by both the AA concentration and the flow rate of the feed. The measured limiting current densities are listed in Table 2 (column 4), and the resultant mass-transfer coefficients of the nine runs of steady-state experiments are evaluated and presented in Table 2 (column 5).

2.4.2. Estimation of model parameters

As stated in Ref. [23], where a DMFC model is studied, the model parameters are difficult to determine directly from experiments. These parameters, as listed in Table 3, are k_1^0 K_1, k_2^0, α and β. The model parameters are estimated in the following manner [24]. Specifically, the model parameters are estimated by minimizing the squared differences of the voltages over six sets of data, namely the quantity F_{obj} defined in Eq. (11) where N is the number of data sets ($N = 6$), and M_i designates the number of data points of the ith data

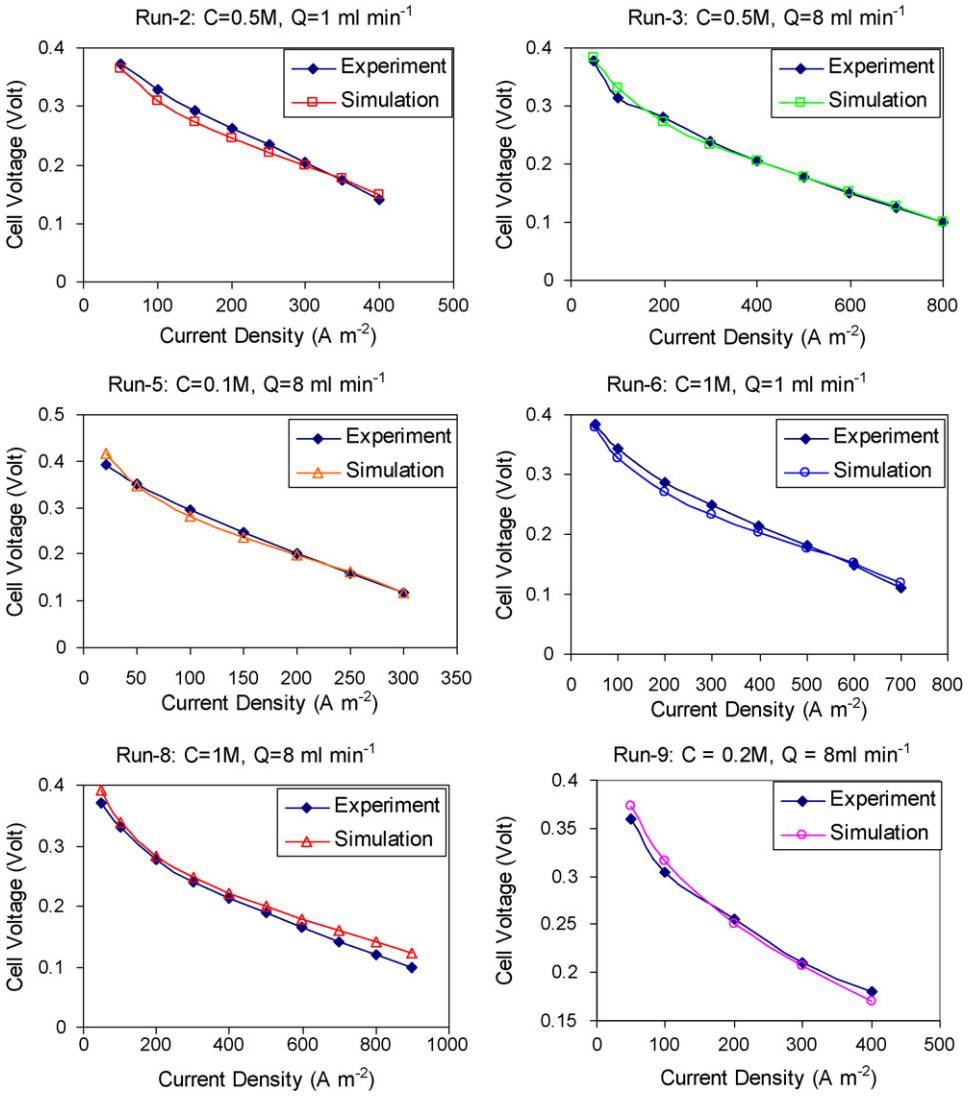

Fig. 2. Comparisons of the experimental measurements and simulated results from best fitting the model using data sets #2, #3, #5, #6, #8, and #9.

Table 4
Average percentage changes in power output due to respective change of each parameter by the factor of 0.9 and 1.1

Ratio	β	C_{AA}^{in}	K^{LS}	k_2^0	α	P_{O_2}	k_1^0	K_1	Q	d^m
0.9	11.6	−5.6	−3.6	−2.5	−2.6	−1.3	−1.2	−0.9	−0.6	0.3
1.1	−13.8	4.0	2.6	2.3	1.9	1.1	1.0	0.8	0.5	−0.3

set.

$$F_{obj} = \sum_{i=1}^{N} \left(\sum_{j=1}^{M_i} \frac{(U_{i,j}^{exp} - U_{i,j}^{cal})^2}{M_i} \right) \quad (11)$$

The simulated cell voltage $U_{i,j}^{cal}$ is obtained from Eq. (9) by solving the system of model Eqs. (1)–(8) at the steady state, i.e., the algebraic equations obtained by setting all the derivatives to zeros. It is noted that six sets of experimental measurements, i.e., sets #2, #3, #5, #6, #8, #9, are used to fit the model and estimate the parameter values, while the remaining three sets, namely #1, #4, #7, serve for validation of the developed model. The resultant parameters are listed in Table 3. Comparisons of the experimental measurements and simulated voltages for the six fitting sets are shown in Fig. 2. As can be seen from the plots, good agreement is observed between the experimental and simulated results generated from the best-fitting model. Furthermore, the model validation is also successful, as shown in the three plots of Fig. 3. The average differences between the experiments and model predictions are in the range of 0.008–0.014 (V), as shown in column 6 of Table 2. It is noted that the differences are generally below the acceptable measurement error of 10% that is equivalent to the minimum measurement error of 0.01 V. Since the three sets of validation data are not involved in fitting the model, it may be concluded that the resulting model demonstrates quite good predictive capability.

3. Results and discussion

3.1. Parameter sensitivity analysis

A primary sensitivity analysis of the operating, design and model parameters was investigated by varying each parameter in turn, while leaving the other parameters unchanged. The average percentage changes in the power output over a range of cell current density of 50–700 (A m^{-2}) are listed in Table 4, where each parameter is varied by 10%. In other words, the parameter is respectively multiplied by a ratio of 0.9 and 1.1 to its original value at the base case, i.e., the experimental condition. As shown in Table 4, when the parameter is reduced by a factor of 0.9, the electron-transfer coefficient of cathode, β, results in the largest boost in power density by an average of 11.6% over the entire range of cell current density. The next largest change is the AA feed concentration which results in a decrease of 5.6%. The mass transfer coefficient K^{LS} ranks the third significant factor which causes a 3.6% decrease in power output. The order of significance of the parameters, as shown by the absolute values of the percentages, is listed in Table 4 with the highest on the left and the lowest on the right. It is noted that in the case of a reduction of parameters, only β and membrane thickness lead to an increase in power output, while others decrease it. On the other hand, the order of parameter significance remains almost unchanged as the parameters are increased by a factor of 1.1, but opposite changes in power generation are observed. In both cases, the membrane thickness is the least significant. A visual examination of the resultant power output due to changes in all the parameters can be found in Fig. 4. As can be seen, higher current densities results in larger deviations from the base case.

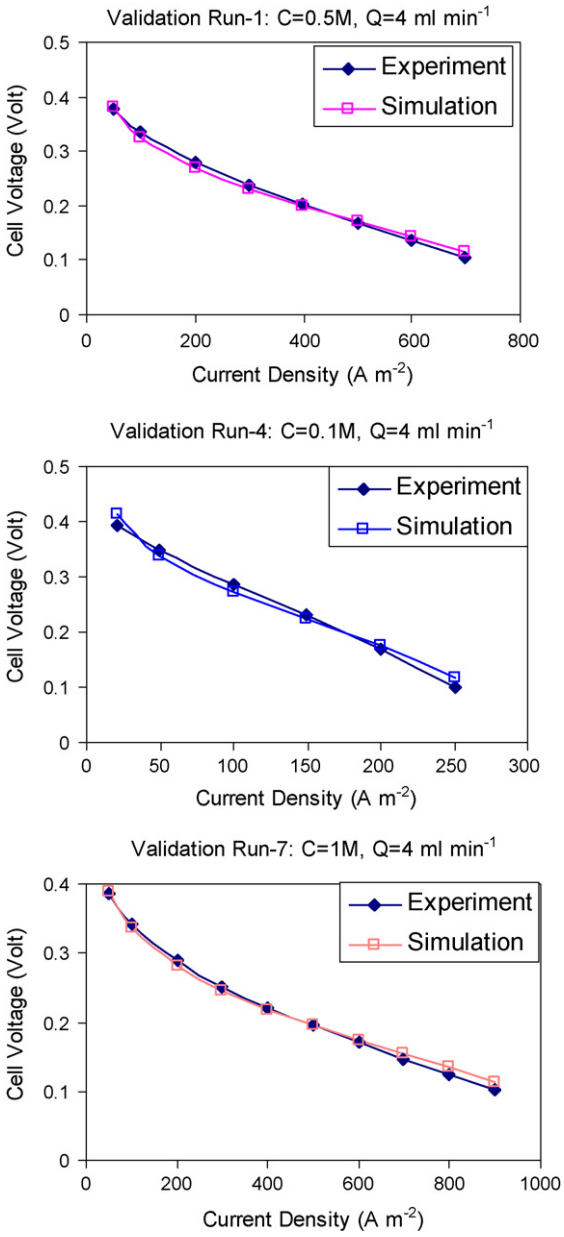

Fig. 3. Model validation by comparing the experimental measurements and the model predictions using data sets #1, #4, #7.

The sensitivity of the five model parameters listed in Table 3 was carried out by the local relative sensitivity analysis method [25], to evaluate the ratio of changes in the computed power density to changes in the parameter values. The following equation was used for the five model parameters.

$$T_j = \frac{P(t, x_j + \delta x_j) - P(t, x_j)}{\delta x_j} \times \frac{x_j}{P(t, x_j)} \qquad j = 1, \ldots, 5 \quad (12)$$

where T_j is time-dependent sensitivity of the jth parameters; x_j is the value of the jth parameter; δx_j is the change in x_j; P is the power density. In the present study, $\delta x_j = 5\% x_j$. A dynamic simulation of step changes in AA feed flow rate from 8 to 4 and then back to 8 ml min^{-1} was conducted to examine the sensitivities of the five parameters. The higher the sensitivity of the parameter, the farther the sensitivity curve locates, apart from zero. As shown in the results (Fig. 5), β sensitivity is the farthest and stands out from all of the rest. Again, this indicates that β is the most sensitive

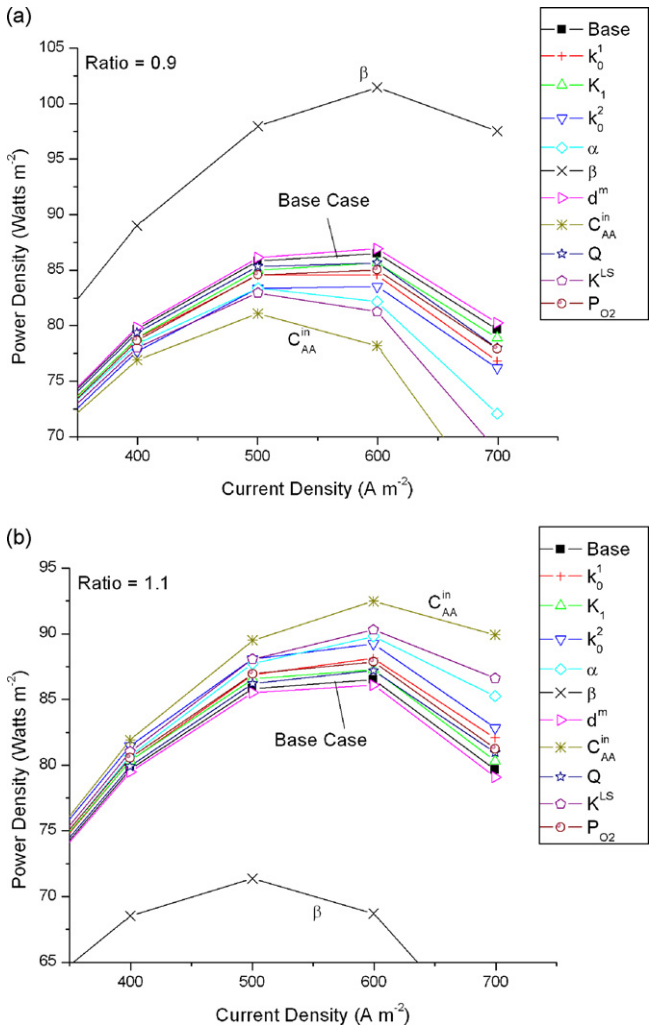

Fig. 4. The power density resulted from (a) decrease in parameters by the factor of 0.9 and (b) increase in parameters by the factor of 1.1.

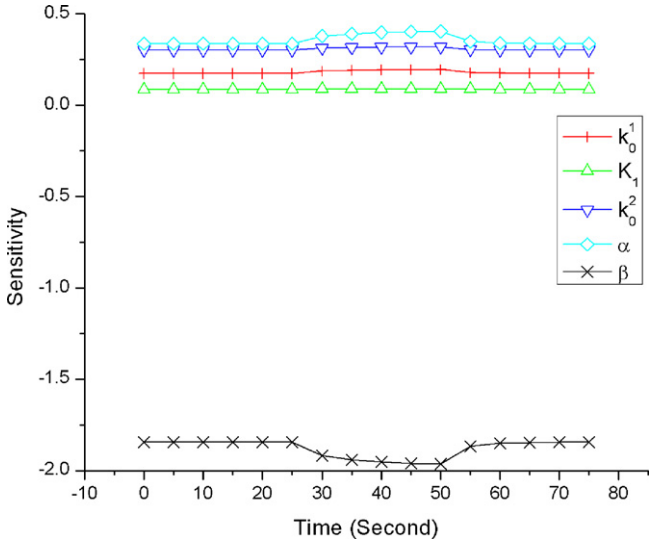

Fig. 5. Result of sensitivity analysis of model parameters.

parameter. The order of the sensitivity of the remaining four parameters (from highest to the lowest) is $\alpha > k_2^0 > k_1^0 > K_1$. Overall, the cathodic reaction is the most significant factor limiting the cell performance, followed by the AA feed concentration and mass-transfer coefficient.

3.2. Steady-state analysis

With the resulting parameters estimated in Section 2.4, the component concentrations and overpotentials of the anode and cathode were evaluated with respect to the changes in cell current density. Since the resultant trends of each run of simulation are similar, only the results from run #1 are presented in this paper. As shown in Fig. 6a, the AA concentrations in both the anode compartment and the catalyst layer linearly decrease with an increase in cell current density, whereas the DHA concentrations increase linearly. This can be explained by the fact that higher current density leads to a larger reaction rate, i.e., faster consumption of the reactant AA and production of DHA. Furthermore, the AA concentration in the compartment is higher than that in the catalyst layer due to the mass-transfer limitation. For the same reason, the DHA generated in the catalyst layer demonstrates opposite trends to those of AA concentration. In Fig. 6b, it is shown that the anode overpotential increases while the cathode overpotential decreases with respect to an increase of current density. These results explain the decrease of cell voltages (Fig. 2).

As mentioned in the preceding section, the fuel (AA) feed concentration is the second significant factor affecting power generation. We therefore studied further the concentration effect by simulation. In particular, the simulation was performed with the AA feed concentration varying from 0.1 to 1.9 M while the flow rate remained unchanged at 4 ml min^{-1} and other parameters also remained unchanged. It is observed in Fig. 7a that the power density increases with increase in fuel feed concentration, and the attainable current density range also increases. The optimum current density that results in maximum power density with respect to the fuel feed concentration is plotted in Fig. 7b.

3.3. Dynamic analysis

3.3.1. Step changes

In this work, we have studied the dynamic behaviour of the DAAFC by simulation and then compared the results with those from experiments. Specially, step changes in AA feed concentration and flow rate are carried out respectively. For the former case, a step decrease in AA feed concentration occurs from 0.5 to 0.2 M at time = 100 s with a flow rate of AA feed at 8 ml min^{-1} and the current density maintained at 100, 200 and 300 A m^{-2}, respectively. Operation prior to the step change (i.e., C = 0.5 M) is equivalent to the steady-state run #3. The simulation and experiment results are given in Fig. 8a. In general, the model is able to simulate the experiment although deviations are found. For instance, a relatively larger discrepancy is observed at current density of 100 A m^{-2}. It is noted that the discrepancy results from fitting the model parameters with all the six sets of experimental readings. As can be seen from the fitting result of run #3 (C = 0.5 M and flow rate = 8 ml min^{-1}) in Fig. 8b that is reproduced from Fig. 2, point A which corresponds to A in Fig. 8a is not well fitted. In fact, point A appears somewhat anomalous in the set of experimental readings that, otherwise, are quite smooth. Therefore, the less consistent fitting of experiment and simulation may lead to the observed discrepancy in the step-change curve. By contrast, point B (200 A m^{-2}) and point C (300 A m^{-2}) are well fitted in Fig. 8b, thus good agreements are observed in the corresponding step-change curves (Fig. 8a). It is noted that there is a valley in each voltage curve, which is due to the practical switch of

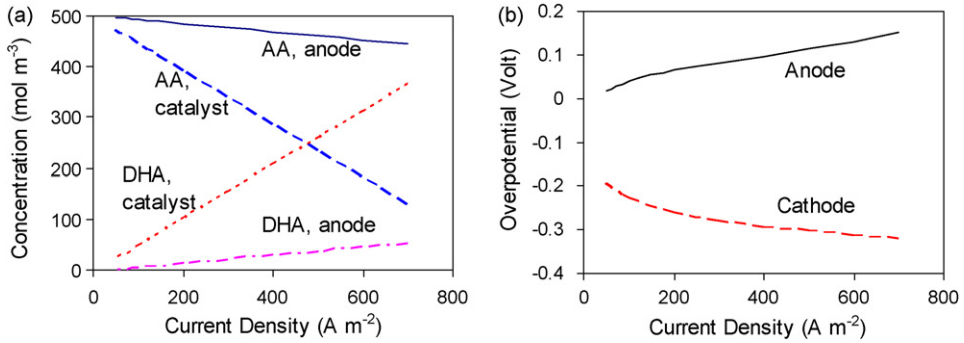

Fig. 6. Steady-state simulation result for run #1. (a) AA and DHA concentrations in anode compartment and catalyst layer and (b) anode and cathode overpotentials.

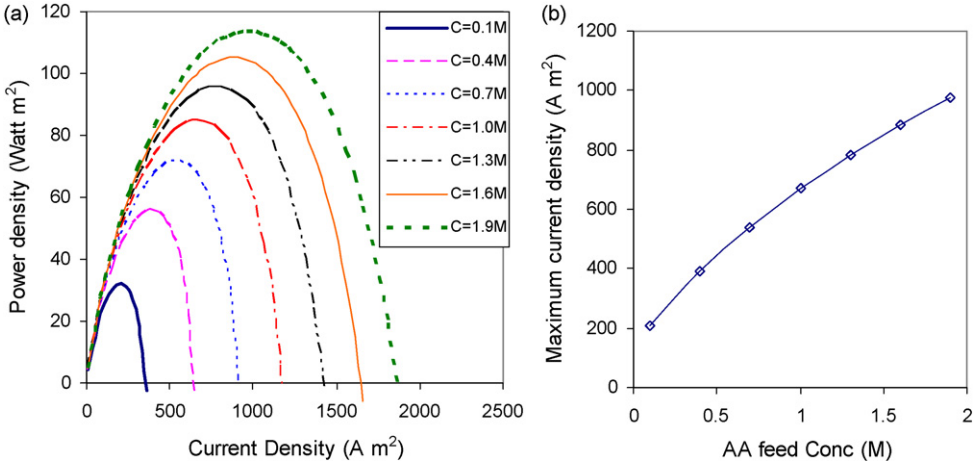

Fig. 7. (a) Simulated power density curves at various AA feed concentrations and (b) maximum power density with respect to different AA feed concentrations.

the feed flow concentration, i.e., in the experiment, the pump was stopped for 5–6 s for each switch.

In the latter case, a step change in AA feed flow rate from 8 to 1 ml min^{-1} was made at time = 50 s, with a constant AA feed concentration of 0.5 M and a current density 200 and 400 A m^{-2}, respectively. This is equivalent to switching from steady-state run #3 to run #2 (see Fig. 2). The simulation and experimental results are shown in Fig. 9a. A minor discrepancy, as shown by point D, can be found for a current density of 400 A m^{-2} before the flow rate is switched. This point is equivalent to point D in Fig. 8b which is the same as the steady-state result shown in Fig. 2 (run #3) where fairly good agreement is observed. Further examination reveals that the discrepancy is caused by the inconsistent results of the two methods of voltage measurement. In other words, all the steady-state I–V data (i.e., run #1 to #9) are measured by a current scan and all the dynamic I–V data by a voltage scan. In this work, the model parameters are estimated by best-fitting all the steady-state measurements, and dynamic data serve as further validation of the

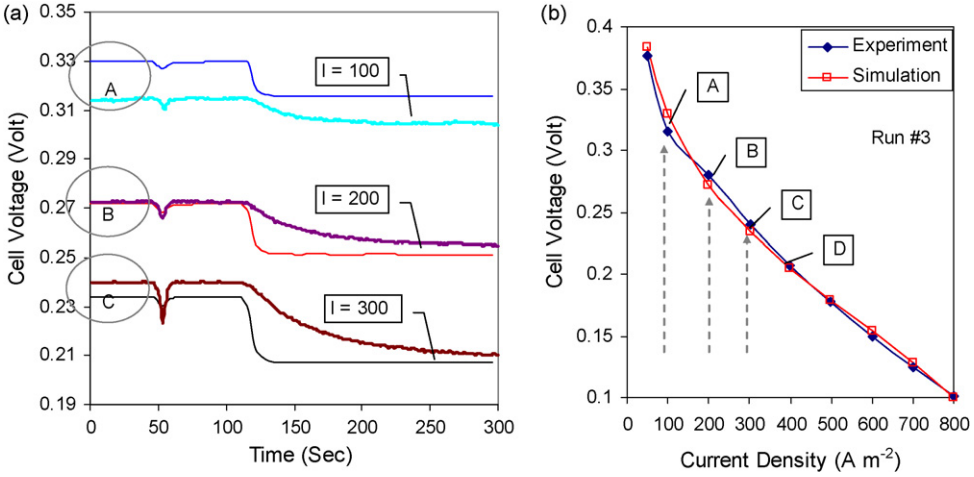

Fig. 8. (a) Comparison of cell voltage of the dynamic simulation (fine lines) and experimental (bold lines) results for the step changes of AA feed concentration from 0.5 to 0.2 M with constant AA feed flow rate of 8 ml min^{-1}. (b) Steady-state simulation and experiment results at AA concentration = 0.5 M and flow rate = 8 ml min^{-1} (run #3).

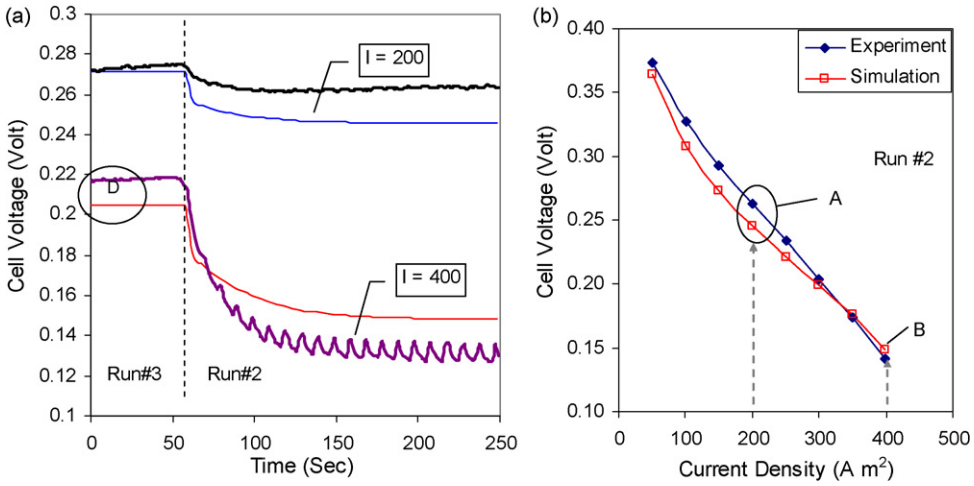

Fig. 9. (a) Comparison of cell voltage of the dynamic simulation (fine lines) and experimental (bold lines) for the step changes of AA feed flow rate from 8 to 1 ml min^{-1} with constant AA feed concentration of 0.5 M. (b) Steady-state simulation and experiment results at AA concentration = 0.5 M and flow rate = 1 ml min^{-1} (run #2).

developed model. This may also explain the discrepancy occurring at 400 A m^{-2} and 1 ml min^{-1} (corresponding to run #2). As seen at point B in Fig. 9b, good agreement is obtained between the simulation and the steady-state experiment as measured by a current scan, but measurements by a voltage scan for the dynamic experiment oscillate and the average is slightly lower than that of the steady state. During 200 A m^{-2} and 1 ml min^{-1} (also corresponding to run #2), the deviation may result from the abovementioned issue or it may inherit from the mismatch during fitting the model parameters at steady state (point A in Fig. 9b).

3.3.2. Periodic changes

In the experiment of periodic dynamics, the delivery pump was switched off at the 18 s point and it took 5–6 s to stop the action completely. The solution was changed from 0.5 M AA to H_2O and the pump was switched on immediately. The water feed started at around 24 s. It is estimated that it took about 2 s to change the fuel solution from 0.5 M AA to water. The fuel solution was changed at 24 s intervals by repeating the above operation. Since the feed solution in the tank approaches the inlet of the fuel cell via three tubes and a pump with a relatively large volume, the switch in fuel solution concentration (from 0.5 M to H_2O) cannot immediately affect the fuel cell operation. In fact, the tubes and pump acted like a buffer. The original AA concentration of the feed can be regarded as unchanged (0.5 M) after the first few switches until the solution in the tubes is replenished. Thus the 0.5-M solution sustains the fuel cell operation for the first few cycles of pump stopping. Thereafter, the solution in the tubes is diluted. The experiments were carried out at current density of 100, 200 and 300 A m^{-2} and the AA flow rate was maintained at 8 ml min^{-1}.

By estimating the volumes of the buffer and the cell, it was found that during the first four cycles AA was fed at 0.5 M. Because of the presence of a buffer to the AA feed flow, the concentration was switched from 0.5 M to an average diluted value, which was calculated as 0.44 M. A comparison of the simulation and experimental results is shown in Fig. 10. The simulation tracks the periodic changes in the voltage curves, but in a more stable fashion. A relatively large deviation is found at a current density of 100 A m^{-2} and is thought to be due to a previous mismatch in fitting the steady state (point A in Fig. 8b). It is observed that some experiment measurements demonstrate very sharp valleys while the simulation does not generate such results. The very low experimental voltages are probably caused by the very low feed concentration when water is being pumped. It can be envisaged that the concentration

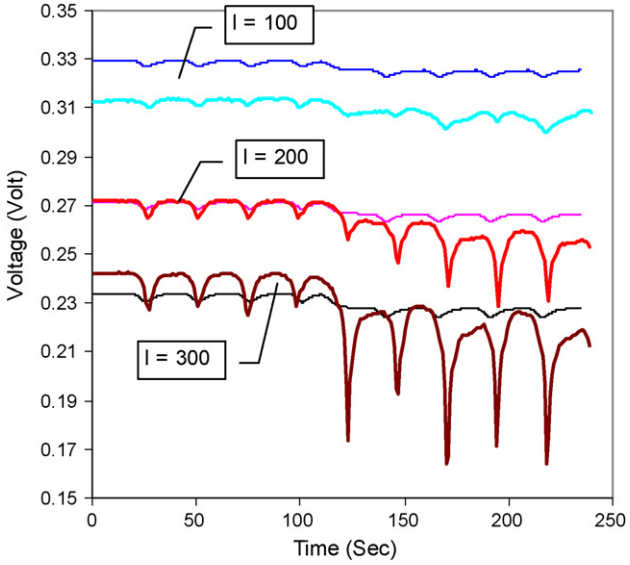

Fig. 10. Comparison of cell voltage of the dynamic simulation (fine lines) and experimental (bold lines) for the periodic changes of AA feed flowrate with constant AA feed flow rate of 8 ml min^{-1}.

change prior to the inlet of the cell is quite complicated and depends not only on the amount of the water but also on the geometry of the buffer space. Since the focus has been on modelling of the fuel cell unit rather than of the feeding facilities, we cannot capture the patterns in feed concentration. In this work, the average feed concentration has been taken for the calculation and thus very low voltages are not predicted.

4. Conclusions

The present work demonstrates a modelling method to describe direct ascorbic acid fuel cells (DAAFCs). In general, the simulation results agree with the experimental data at steady or dynamic states. Since the present study focuses only on the fuel cell itself, however, changes in the feed flow concentration prior to approaching the inlet cannot be accurately simulated. Furthermore, the assumption of ideal mixing in the anode compartment may also cause less accurate prediction because the anode is a narrow and relatively long channel. As a result, the transient behaviour of the

simulated voltages does not completely match that of experiments at the points where a step change occurs.

The parameter sensitivity analysis by simulation reveals that the cathode electron transfer coefficient β is the most significant factor limiting the cell performance, followed by the AA feed concentration C_{AA}^{in} and mass-transfer coefficient K^{LS}. To improve the DAAFC performance by varying β and K^{LS}, the important issues are to develop more efficient cathode materials and catalyst materials. This is, however, beyond the scope of the present study and should be the subject of further investigation. Simulation shows that an increase in C_{AA}^{in} will lead to a boost of the power generation. This result may imply that in order to obtain higher power generation, the AA feed concentration should be increased as high as possible. The present investigation offers further insight into how various parameters affect the power output, and may provide guidance for more efficient DAAFC design and operational strategies.

References

[1] P. Costamagna, S. Srinivasan, J. Power Sources 102 (2001) 242–252.
[2] E. Antolini, Appl. Catal. B: Environ. 74 (2007) 324–336.
[3] K. Sundmacher, T. Schultz, S. Zhou, K. Scott, M. Ginkel, E.D. Gilles, Chem. Eng. Sci. 56 (2001) 333–341.
[4] V. Neburchilov, J. Martin, H.J. Wang, J.J. Zhang, J. Power Sources 169 (2007) 221–238.
[5] M.J. Valls, J.M. Feliu, A. Aldaz, M.A. Climent, J. Clavilier, J. Electroanal. Chem. 260 (1989) 237–244.
[6] X. Xing, I.T. Bae, M. Shao, C.C. Liu, J. Electroanal. Chem. 346 (1993) 309–321.
[7] S.K. Mondal, R.K. Raman, A.K. Shukla, N. Munichandraiah, J. Power Sources 145 (2005) 16–20.
[8] N. Fujiwara, S. Yamazaki, Z. Siroma, T. Ioroi, K.I. Yasuda, Electrochem. Commun. 8 (2006) 720–724.
[9] N. Fujiwara, Z. Siroma, T. Ioroi, K. Yasuda, J. Power Sources 164 (2007) 457–463.
[10] S. Zhou, T. Schultz, M. Peglow, K. Sundmacher, Phys. Chem. Chem. Phys. 3 (2001) 347–355.
[11] N. Fujiwara, S. Yamazaki, Z. Siroma, T. Ioroi, K. Yasuda, J. Power Sources 167 (2007) 32–38.
[12] A. Biyikoglu, Int. J. Hydrogen Energy 30 (2005) 1181–1212.
[13] W.W. Yang, T.S. Zhao, C. Xu, Electrochim. Acta 53 (2007) 853–862.
[14] U. Krewer, A. Kamat, K. Sundmacher, J. Electroanal. Chem. 609 (2007) 105–119.
[15] V.B. Oliveira, D.S. Falcao, C.M. Rangel, A.M.F.R. Pinto, Int. J. Hydrogen Energy 32 (2007) 415–424.
[16] X.L. Li, Y.L. He, B.H. Yin, Z. Miao, X.Y. Li, J. Power Sources 178 (2008) 344–352.
[17] U. Krewer, H.K. Yoon, H.T. Kim, J. Power Sources 175 (2008) 760–772.
[18] C. Spiegel, PEM Fuel Cell Modeling and Simulation Using Matlab, Academic Press, 2008.
[19] E. Fontes, C. Oloman, G. Lindbergh, Handbook of Fuel Cell Modeling, Elsevier Advanced Technology, Oxford, 2004.
[20] MATLAB 7.0. The Mathworks Inc. http://www.mathworks.com.
[21] N. Fujiwara, K. Yasuda, T. Ioroi, Z. Siroma, Y. Miyazaki, T. Kobayashi, Electrochem. Solid-State Lett. 6 (2003) A257–A259.
[22] S. Uhm, J. Choi, S.T. Chung, H. Lee, Electrochim. Acta 53 (2007) 1731–1736.
[23] C. Xu, P.M. Follmann, L.T. Biegler, M.S. Jhon, Comput. Chem. Eng. 29 (2005) 1849–1860.
[24] Y. Zeng, S.J. Mu, S.J. Lou, B. Tartakovsky, S.R. Guiot, P. Wu, Biochem. Eng. J. 25 (2005) 113–123.
[25] A. Saltelli, K. Chan, E.M. Scott, Sensitivity Analysis, John Wiley and Sons, New York, 2000.